NANO LETTERS

pubs.acs.org/NanoLett Letter

Electric Control of Exchange Bias Effect in $FePS_3$–Fe_5GeTe_2 van der Waals Heterostructures

Sultan Albarakati,[#] Wen-Qiang Xie,[#] Cheng Tan,[#] Guolin Zheng,[*] Meri Algarni, Junbo Li, James Partridge, Michelle J. S. Spencer, Lawrence Farrar, Yimin Xiong, Mingliang Tian, Xiaolin Wang, Yu-Jun Zhao,[*] and Lan Wang[*]

Cite This: *Nano Lett.* 2022, 22, 6166–6172 Read Online

ACCESS | Metrics & More | Article Recommendations | Supporting Information

ABSTRACT: Manipulating the exchange bias (EB) effect using an electronic gate is a significant goal in spintronics. The emergence of van der Waals (vdW) magnetic heterostructures has provided improved means to study interlayer magnetic coupling, but to date, these heterostructures have not exhibited electrical gate-controlled EB effects. Here, we report electrically controllable EB effects in a vdW heterostructure, $FePS_3$-Fe_5GeTe_2. By applying a solid protonic gate, the EB effects were repeatably electrically tuned. The EB field reaches up to 23% of the coercivity and the blocking temperature ranges from 30 to 60 K under various gate-voltages. The proton intercalations not only tune the average magnetic exchange coupling but also change the antiferromagnetic configurations in the $FePS_3$ layer. These result in a dramatic modulation of the total interface exchange coupling and the resultant EB effects. The study is a significant step toward vdW heterostructure-based magnetic logic for future low-energy electronics.

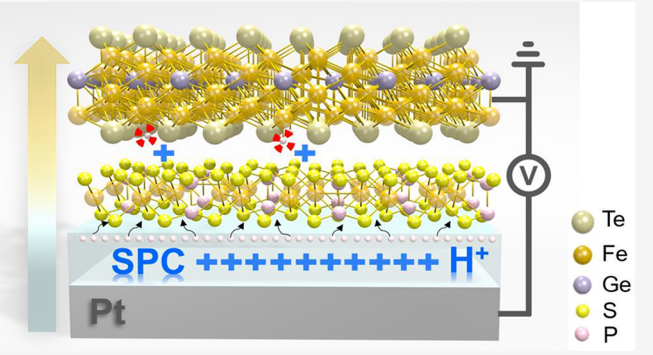

KEYWORDS: *gate-tuned exchange bias effect, $FePS_3$–Fe_5GeTe_2 van der Waals heterostructures, interlayer magnetic coupling, proton intercalation*

The exchange bias (EB) effect, originating from antiferromagnetic(AFM)–ferromagnetic (FM) interface coupling induced unidirectional anisotropy, has played a significant role in fundamental magnetic and spintronic device applications[1−6] since its discovery.[7] As a long time pursuit for spintronics applications, electrical gate-manipulated EB effects in AFM–FM structures enable scalable energy-efficient spin–orbit logic, which is very promising for beyond-COMS devices in future low energy electronic technologies.[8] To date, only very limited electrically tunable EB effects have been experimentally demonstrated, and most of them have been based on oxide multiferroic thin film systems.[9−12] The recent emergence of van der Waals (vdW) heterostructures[13−15] and the discovery of 2D ferromagnetism[16,17] have enabled various studies on vdW magnetic and spintronic devices.[18−20] The high-quality interfaces and weak interlayer coupling observed in vdW magnetic heterostructures so far suggest opportunities to explore intrinsically interfacial magnetic coupling mechanisms. This is in contrast to coupling in traditionally grown thin films, which tends to be governed largely by interfacial defects.[21−24] Despite EB effects being extensively investigated in vdW magnets and AFM–FM heterostructures,[25−30] an electrically tunable EB effect in vdW AFM–FM heterostructures has yet to be realized. A recent study[31] has demonstrated that solid protonic gates are effective tools for manipulating the interlayer magnetic coupling in single-crystalline Fe_3GeTe_2. Hence, this motivates the application of solid protonic gates to vdW AFM–FM heterostructures with the aim of electrically tunable EB in vdW AFM–FM heterostructures.

Here, for the first time, we largely tuned the EB effects electrically in vdW AFM–FM heterostructures using a solid protonic gate. $FePS_3$(AFM)–Fe_5GeTe_2(FM, F5GT) vdW heterostructure is used as a model system that shows strong interface magnetic coupling at the AFM–FM interfaces. Notably, unlike in Fe_3GeTe_2, the proton intercalation cannot result in exchange bias in a single F5GT layer with various thicknesses (see Supporting Information Section 1.5 and Figure S8).[32] This coupling gives rise to a large EB effect that is influenced by the thickness of the Fe_5GeTe_2 layer and the amplitude of the cooling field $H_{cooling}$. It is insensitive to the

Received: April 6, 2022
Revised: July 22, 2022
Published: July 31, 2022

https://doi.org/10.1021/acs.nanolett.2c01370
Nano Lett. 2022, 22, 6166–6172

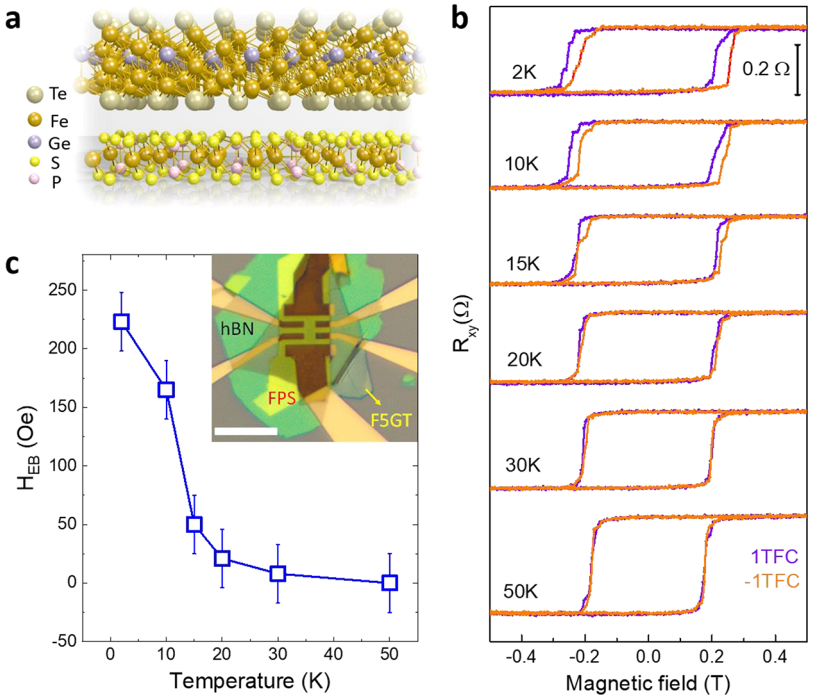

Figure 1. EB effects in a FPS−F5GT vdW heterostructure (device #2) without gating. (a) Schematic of the FPS−F5GT heterostructure. (b) Temperature-dependent EB effects in device #2 under cooling fields of ±1 *T*. (c) Amplitudes of the EB effects at various temperatures. Inset: optical image of device #2. Scale bar: 10 μm. All loops are vertically shifted for clarity. The error bars are defined by the field error in MPMS3 system (Figure S7), same as below.

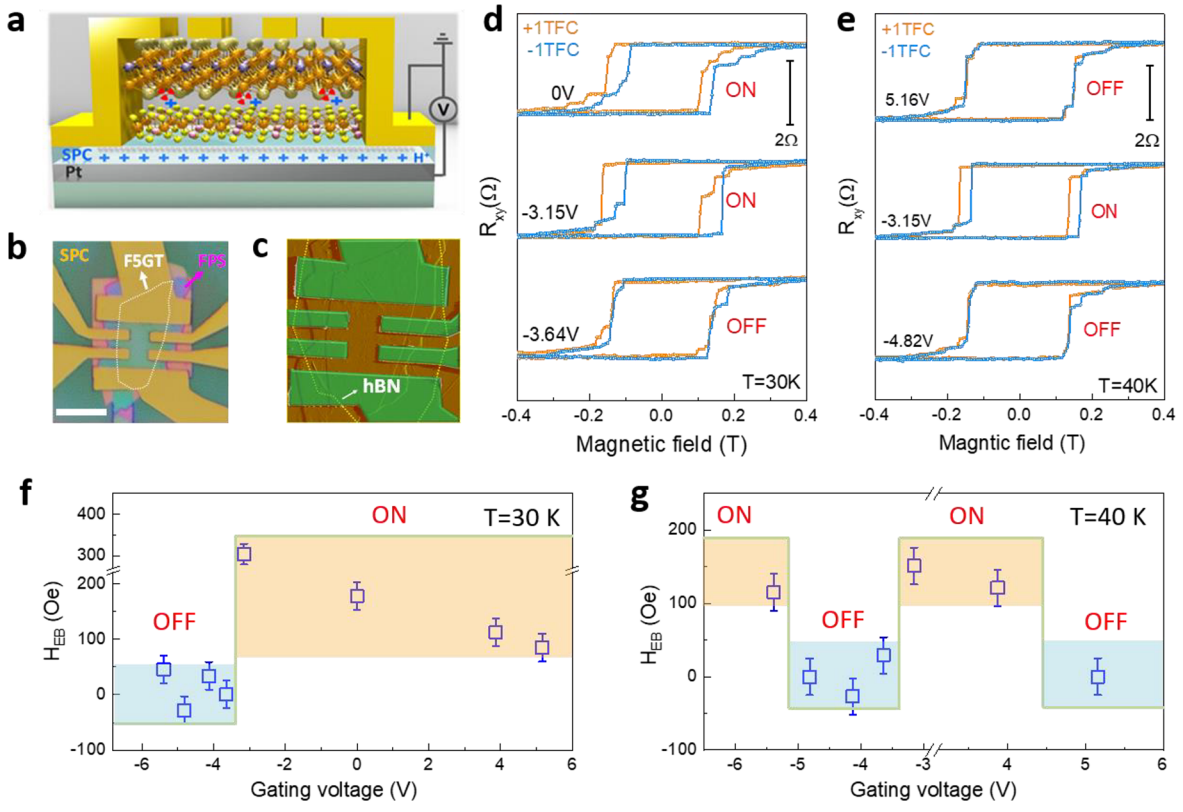

Figure 2. Gate tunable EB effects in the FPS−F5GT vdW heterointerfaces (device #3). (a) Schematic of the solid proton field effect transistor (SP-FET). (b, c) Optical and atomic force microscope images of device #3. Scale bar: 10 μm. (d, e) Gate-dependent EB effects at T = 30 and 40 K, respectively. (f, g) Amplitudes of the EB effects under various gating voltages at T = 30 and 40 K, respectively. All loops are vertically shifted for clarity.

thickness of the $FePS_3$ (FPS) layer (≥15 nm). Specifically, the EB effects are only observed in FPS−F5GT heterostructures within a small cooling field (≤2 T) and a narrow FM thickness range of 10 to 20 nm. Theoretical analysis using density

https://doi.org/10.1021/acs.nanolett.2c01370
Nano Lett. 2022, 22, 6166−6172

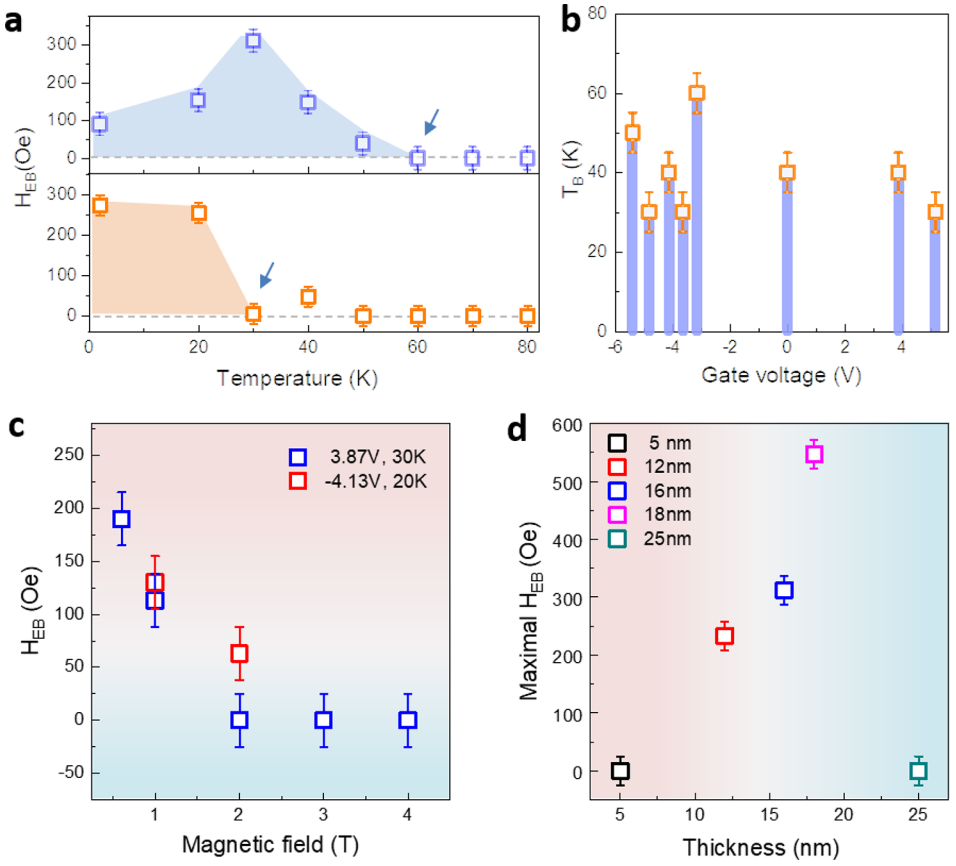

Figure 3. Dependence of the EB effects on temperature, voltage, cooling field, and thickness. (a) Temperature-dependent EB effects at selected gate voltages in device #3. (b) Gate-dependent blocking temperature T_B in device #3. (c) Cooling field-dependent EB effects in device #3. A large cooling field can significantly suppress the EB effects. (d) Thickness (F5GT)-dependent maximum EB field. The EB effects were only exhibited in F5GT with thickness between 10 and 20 nm.

functional theory indicates that the proton intercalations affect the FPS−F5GT heterostructures in two significant ways. First, by intercalating the protons into the FPS−F5GT interface, the average interlayer exchange coupling J_{ij} can be tuned. Second, intercalation can also change the AFM configurations in the FPS layer and transform the FPS−F5GT heterointerface from an uncompensated AFM−FM interface to a compensated AFM−FM interface. This modulation of the AFM configurations results in a dramatic change of the total interface magnetic coupling J_{int} and the resultant EB effects. This realization of electrically controllable EB effects in a vdW AFM−FM heterostructure represents a significant step toward enabling vdW heterostructure-based magnetic logic for lower energy electronics.

In our AFM−FM heterostructures, the FM layer, F5GT, is a vdW ferromagnet with a Curie temperature, T_c of 300 K in bulk.[33] The F5GT crystal is formed from thicker Fe−Ge slabs sandwiched by Te layers. The crystal structure of F5GT has a space group $R3m$ with lattice parameters a = 4.04 Å and c = 29.19 Å. The AFM layer, FPS, has a monoclinic structure with the space group of $C2/m$. FPS is an Ising-type AFM with a Néel temperature $T_N \approx 123$ K.[34,35] Figure 1a shows a schematic of our heterostructure device. During its construction, a FPS layer was first stacked onto a F5GT layer to form an AFM−FM heterostructure. The heterostructure was then covered by a hBN layer and transferred onto Pt contacts of thickness ∼15 nm (see the inset of Figure 1c, device #2). Figure 1b shows temperature-dependent EB effects in device #2 (with thicknesses t_{F5GT} = 12 nm, $t_{FPS} \approx$ 20 nm) observed under cooling fields $H_{cooling} = \pm$ 1 T. In this study, the magnetic fields were always applied perpendicular to the devices' surfaces. After field cooling from 150 K ($>T_N$), the hysteresis loops at low temperatures shifted to the opposite directions of the cooling fields, thus producing negative EB effects (Figure 1b). As the temperature was increased, the EB fields ($H_{EB} = |H_{EB}^{+} + H_{EB}^{-}|/2$) were gradually "smeared out" and were suppressed above the blocking temperature, T_B = 20 K due to thermal fluctuations, as shown in Figure 1c. The emergence of the EB effect below 20 K in device #2 is indicative of a strong magnetic coupling at the FPS−F5GT interface.

To further explore the manipulation of the EB effect, protons were intercalated into the FPS−F5GT heterointerfaces using protonic gates. Figure 2a shows a schematic of our gating devices. The FPS−F5GT bilayers were mounted on solid protonic conductors with gating electrodes underneath to form solid proton field effect transistors (SP-FET). Figure 2b shows an optical image of gating device #3, with an upper F5GT layer of thickness t_{F5GT} = 16 nm and lower FPS layer of thickness t_{FPS} = 15 nm. The heterostructure was covered entirely in situ by a thin hBN layer, as shown in the atomic force microscope image in Figure 2c. The gating voltages were applied between the bottom electrode (∼10 nm Pt) and the source electrode. At low temperatures, device #3 exhibited robust EB effects irrespective of the gating voltage (Section 1.1, Supporting Information). However, above 20 K, the EB effects were strongly dependent on the gate voltage. Figure 2d and e illustrate the gate-dependent

https://doi.org/10.1021/acs.nanolett.2c01370
Nano Lett. 2022, 22, 6166−6172

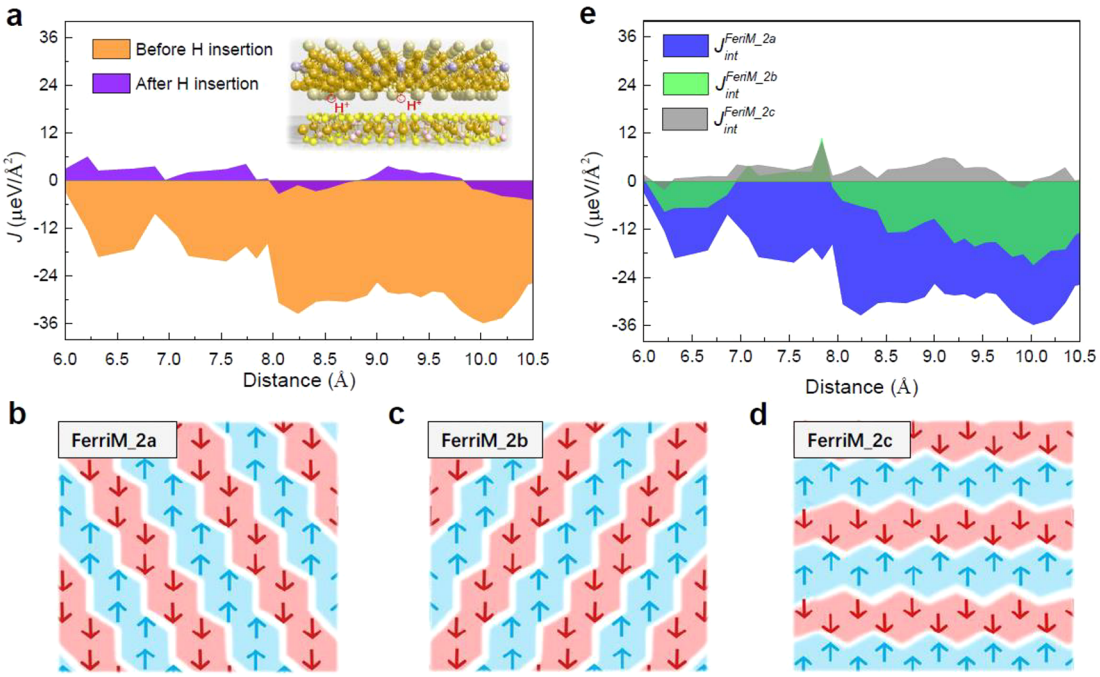

Figure 4. Theoretical analysis based on DFT. (a) Calculated interface magnetic couplings before (FPS/F5GT-up model) and after insertion of a H atom (FPS/H/F5GT-up-1 model) with a magnetic configuration of FerriM_2*a*. (b, c, d) Illustrations of three equivalent magnetic configurations of the FPS layer in the interface. That is, FerriM_2*a*, FerriM_2*b*, and FerriM_2*c*. *a*, *b*, and *c* represent three different zigzag orientations. The blue areas indicate "spin up", while the red ones suggest "spin down". (e) Calculated interface magnetic couplings of the FerriM_2*a*, FerriM_2*b*, and FerriM_2*c* configurations with the FPS/F5GT-up model.

EB effects observed in device #3 at T = 30 and 40 K, respectively. At T = 30 K, device #3 exhibited large interface magnetic coupling with a distinct negative EB effect (H_{EB} = 178 Oe) at V_g = 0 V. Here, when $|H_{EB}| > 50$ Oe, the EB effect is regarded as an "ON" state, while an "OFF" state occurs when $|H_{EB}| \leq 50$ Oe. The critical H_{EB} = 50 Oe is defined by the magnetic field error due to the flux pinning effect in the superconductor magnet (see Supporting Information Section 1.4 and Figure S7). By applying a negative voltage bias of −3.15 V, the EB effect became more prominent with a maximum EB field H_{EB} = 310 Oe, reaching 23% of the coercivity (H_{EB}/H_C = 23%). However, the EB effect vanished abruptly when the voltage bias was swept to −3.64 V, indicating suppression of the interface magnetic coupling and providing an "OFF" state. This absence of the EB effect within such a small gate voltage interval is indicative of the sensitivity of the interface magnetic coupling to proton intercalations or deintercalations. Figure 2f shows the EB amplitudes under different gate voltages measured at 30 K. Specifically, the EB effects could be regarded as turning "ON" for $V_g \geq -3.15$ V and turning "OFF" for $V_g < -3.15$ V. Similar phenomena were recorded at T = 40 K. There was no EB effect with V_g = 5.16 V at T = 40 K, as shown in Figure 2e, indicating negligible interface magnetic coupling. However, the EB effect re-emerged at V_g = −3.15 V with a magnitude of H_{EB} = 151 Oe, once again representing an "ON" state of interface magnetic coupling. Sweeping the gate voltage again to V_g = −4.82 V, the EB effect vanished again and hence an "OFF" state was realized. Figure 2g shows that consecutively sweeping the gate voltages from −5.39 to 5.16 V caused alternate emergence ("ON") and suppression ("OFF") of the EB effects.

The highly tunable nature of the EB effects was made further apparent when observing the gate-dependent blocking temperature T_B. Specifically, no EB effect was detected with $T > 50$ K, indicating a T_B of approximately 60 K at V_g = −3.15 V in device #3. However, T_B dropped to 30 K at −3.64 V, as shown in Figure 3a. By consecutively changing the gate voltages, we found that T_B varied between 30 and 60 K, as illustrated in Figure 3b. Compared to the low blocking temperature exhibited in device #2 (~20 K) without gating, the much higher blocking temperature in device #3 obtained at −3.15 V shows that the interlayer magnetic coupling was effectively controlled by the protonic gating. Besides their strong dependence on gate voltage, the EB effects were also found to be substantially suppressed under large cooling fields, as shown in Figure 3c. In device #3 with T = 20 K and V_g = −4.13 V, a small cooling field of $H_{cooling}$ = 1 T generated a negative EB effect with an amplitude of about 126 Oe. However, when the cooling field was increased to $H_{cooling}$ = 2 T, the EB field decreased to around 60 Oe (shown as red, open squares). A similar trend was also observed in device #3 with T = 30 K and V_g = 3.87 V. For a small cooling field of $H_{cooling}$ = 0.6 T, a large EB effect was observed with $H_{EB} \approx 190$ Oe. However, as the cooling field increased, the EB effects gradually decreased, and they were negligible when the cooling field $H_{cooling} > 2$ T (shown as blue open squares in Figure 3c). The dependence of EB effects on the thickness of the FM layer (shown in Figure 3d) was revealed in experiments in which the FPS thickness t_{FPS} was maintained at less than 15 nm while the thickness of the F5GT, t_{F5GT}, was varied. EB effects were observed in the FPS−F5GT heterostructures with t_{F5GT} = 12 nm (device #2), 16 nm (device #3), and 18 nm (device #4). Among them, a maximum EB effect reaching $H_{EB} \approx 570$ Oe was detected in device #4 at 2 K with V_g = 2.82 V (Section 1.2, Supporting Information). However, no EB effects were observed in device #1 (t_{F5GT} = 5 nm) and device #5 (t_{F5GT} = 25 nm), as shown in Figure 3d (also in Section 1.2, Supporting Information). Devices #1, #3, #4, and #5 were mounted on protonic conductors, while

https://doi.org/10.1021/acs.nanolett.2c01370
Nano Lett. 2022, 22, 6166−6172

device #2 was mounted on a SiO_2 substrate without a protonic conductor. The EB effect is regarded as an interface effect and would be expected to diminish if the thickness of the FM layer was increased. Our experimental observations are consistent with this, showing no occurrence of EB effects when $t_{F5GT} > 20$ nm. However, EB effects were also absent in heterostructure devices with thinner F5GT nanoflakes ($t_{F5GT} < 10$ nm), even under protonic gating. This latter observation is attributed to the extremely large coercivity ($H_C \approx 2$ T) characteristic of the thinner F5GT nanoflakes (<10 nm) arising from intralayer defect pinning.[32] The energy barrier induced by defect pinning is significantly larger than that from unidirectional anisotropy. Thus, the magnetic field required to overcome the pinning effect in the magnetization process would be sufficient to overwhelm the unidirectional anisotropy induced by the interface magnetic coupling and thereby suppress EB effects.

To gain more insight into the gate-dependent EB effects, a theoretical analysis using density functional theory (DFT) was performed.[36,37] The computational details are included in Section 2 of the Supporting Information. In brief, the heterojunction models were constructed as follows. First, 12 different displaced combinations between FPS and F5GT were analyzed (Figure S9). The combination with the lowest adhesion energy (FPS/F5GT-up model) was then chosen for further calculations. Second, the adsorption sites of H in a single layer and heterojunction were optimized, and the structure with the lowest adsorption energy (FPS/H/F5GT-up-1 model) was selected for analysis (Figures S10 and S11). Finally, possible AFM magnetic configurations of the FPS layers were examined within our constructed heterointerfaces (Figure S12).

Generally, the EB effect depends strongly on the interface coupling of AFM−FM system[38] and it is difficult to generate using an Ising-type AFM because the interface is highly compensated.[39] The intensity of the EB effect relates to the difference of two neighboring domains ($\Delta\sigma$).[39] For an ideally uncompensated AFM−FM coupling system, $\sigma = \pm J_{int}/a_{lat}^2$, where a_{lat} is the lattice parameter. J_{int} is the total interface exchange coupling and is equal to the integrated average magnetic exchange coupling (J_{ij}) up to a given distance (Section 2.1, Supporting Information). For an ideally compensated system, $\sigma = J_{int} = 0$. In a F5GT/FPS heterostructure, due to the low $P1$ symmetry of the heterojunction, the interface is uncompensated, giving rise to a nonzero EB effect. The EB effect may be influenced by three factors, namely the exchange coupling J_{ij} at the heterointerface and the magnetic states of F5GT and FPS. According to our previous experimental study,[32] the protonic-gate cannot generate exchange bias in a single F5GT layer, and F5GT nanoflakes with $t_{F5GT} < 20$ nm also retain their ferromagnetic states under a protonic gates. Hence, the influence of protonic gate on F5GT layer is negligible, and the effect of interlayer coupling between FPS−F5GT and the AFM configurations in FPS alone is important in explaining our experimental results. We obtained two key results from our DFT calculations (Sections 2.4−2.6, Supporting Information). First, the interlayer coupling at the FPS−F5GT interface decreases as proton intercalation increases. As shown in Figure 4a, after intercalating H into the FPS−F5GT interface, the average magnetic exchange coupling J_{ij} is decreased or reversed (Sections 2.4 and 2.6, Supporting Information), resulting in a dramatic suppression of total interface magnetic coupling J_{int}. Second, FPS has several equivalent AFM configurations with small energy differences. Both a protonic gate and a magnetic field can induce a phase transition between an uncompensated AFM and a compensated AFM state (Section 2.5, Supporting Information). The three energy-favored equivalent configurations of the FPS layer FerriM_2*a*, FerriM_2*b*, and FerriM_2*c* are shown in Figure 4b, c, and d, respectively. As illustrated in Figure 4e, the magnetic coupling energies $J_{int}^{FerriM\_2b}$ and $J_{int}^{FerriM\_2c}$ are significantly suppressed compared with $J_{int}^{FerriM\_2a}$, suggesting that magnetic transformations between equivalent AFM configurations could also lead to a significant decrease in interface coupling (strong compensation).

On the basis of the two aforementioned key results, gate-dependent EB effects can be well explained. In Figure 2, the protons can be intercalated into the FPS−F5GT interface at $V_g > 0$ V, which decreases the interface coupling. Hence, the "OFF" state around $V_g = +5.16$ V at 40 K is due to the small interface coupling after H insertion. Around 5.16 V, the thermal agitation energy at 40 K is larger than the AFM−FM coupling induced unidirectional anisotropy energy and hence EB disappears. EB values increase from +5.16 V to −3.15 V at 30 and 40 K (also in Figure S2) due to the deintercalation of the protons.

The transition from the "ON" state to the "OFF" state at around −3.15 V can be attributed to the phase transition of FPS from an uncompensated AFM state (between +5.16 V and −3.15 V) to a compensated AFM state ($V_g < -3.15$ V at 30 K and -4.82 V $< V_g < -3.15$ V at 40 K). A similar phase transition from a compensated AFM state to an uncompensated AFM state occurs in the FPS again at around −5.39 V at 40 K, leading to an "ON" state. Now we explain the variation of T_B in Figure 3a and b. At $V_g > -3.15$ V, T_B is mainly determined by the interface exchange J_{ij} of FPS−F5GT (Section 2.4, Supporting Information). Intercalating the protons into the interface decreases the interface coupling, resulting in a decrease of T_B at $V_g > 0$ V. At $V_g < -3.15$ V; however, the transformation of FPS between an uncompensated AFM and a compensated AFM leads to a decrease (at -4.82 V $< V_g < -3.15$ V) or an increase (at −5.39 V) of T_B. Note that the magnetic structure can also be tuned by the magnetic field,[25,40] which may lead to a magnetic transition from an uncompensated AFM to a compensated AFM in FPS. The compensated AFM is more stable in FPS at high magnetic fields, which explains the disappearance of the EB at 30 K when $|H_{cooling}| > 2$ T, as shown in Figure 3f.

In conclusion, electrically tunable exchange bias effects in the vdW FPS−F5GT heterostructures have been reported. These originate from interface magnetic coupling in the vdW heterostructures that was tuned via protonic gate intercalation. With the assistance of density functional theory, we determined that the interface exchange coupling is modulated either by direct intercalation of protons into FPS−F5GT interface or by transformations among equivalent AFM configurations in the FPS layer. Our study highlights a potential route toward magnetic logic for beyond-CMOS applications.

Methods. *Single Crystal Growth.* Single crystal FPS and some F5GT single crystals were purchased from HQ graphene. Other F5GT crystals were grown by the transport method discussed in ref 33.

Device Fabrication and Transport Measurements. All hBN, F5GT, and FPS flakes were mechanically exfoliated in a glovebox with oxygen and water levels below 0.1 ppm. We first used a large hBN layer to pick up the FPS layer and then the F5GT layer in situ; the hBN/FPS/F5GT heterostructure was then transferred onto underlying Pt electrodes using a dry transfer technique. For the gating devices, we first used a thin hBN layer (thinner than 3 nm) to pick up the F5GT layer and then FPS layer to form hBN/F5GT/FPS heterostructures.

https://doi.org/10.1021/acs.nanolett.2c01370
Nano Lett. 2022, 22, 6166−6172

These were finally transferred onto the solid proton conductors. Standard electron beam lithography was then used to fabricate the Hall bar devices. Before the Cr/Au evaporation, the top hBN layer in the vicinity of the Hall bar was etched using an Ar plasma for 90 s with an etch rate of ∼4 nm/min. The solid protonic electrolyte was prepared via the sol−gel process (described in ref 31). Protonic gating experiments were performed in a commercial Magnetic Property Measurement System (MPMS) via the electrical transport option (ETO) probe with a maximum magnetic field of 7 T. To decrease the leakage current, the gate voltage was swept at 250 K. Once the resistance change was observed, the device was rapidly cooled to low temperatures for magneto-transport measurements.

■ ASSOCIATED CONTENT

Supporting Information

The Supporting Information is available free of charge at https://pubs.acs.org/doi/10.1021/acs.nanolett.2c01370.

Extended experimental data; extra data in device #3; exchange bias under different thicknesses; tunable ON and OFF states of exchange bias effects in device #6; field error in MPMS3 system; effect of proton intercalation on top F5GT layer; theoretical analysis; computational details; structural modeling of interface; magnetic configuration modeling of interface; interface coupling suppression induced by H insertion; interface coupling suppression induced by magnetic transition of FPS layer; magnetic properties of constructed interface (PDF)

■ AUTHOR INFORMATION

Corresponding Authors

Guolin Zheng − *Anhui Province Key Laboratory of Condensed Matter Physics at Extreme Conditions, High Magnetic Field Laboratory, Chinese Academy of Sciences (CAS), Hefei, Anhui 230031, China*; Email: glzheng@hmfl.ac.cn

Yu-Jun Zhao − *Department of Physics, South China University of Technology, Guangzhou 510640, China*; orcid.org/0000-0002-6923-1099; Email: zhaoyj@scut.edu.cn

Lan Wang − *ARC Centre of Excellence in Future Low-Energy Electronics Technologies (FLEET), School of Science, RMIT University, Melbourne, Victoria 3001, Australia*; orcid.org/0000-0001-7124-2718; Email: lan.wang@rmit.edu.au

Authors

Sultan Albarakati − *ARC Centre of Excellence in Future Low-Energy Electronics Technologies (FLEET), School of Science, RMIT University, Melbourne, Victoria 3001, Australia; Physics Department, Faculty of Science and Arts, University of Jeddah, 21589 Khulais, Saudi Arabia*

Wen-Qiang Xie − *Department of Physics, South China University of Technology, Guangzhou 510640, China*

Cheng Tan − *ARC Centre of Excellence in Future Low-Energy Electronics Technologies (FLEET), School of Science, RMIT University, Melbourne, Victoria 3001, Australia*

Meri Algarni − *ARC Centre of Excellence in Future Low-Energy Electronics Technologies (FLEET), School of Science, RMIT University, Melbourne, Victoria 3001, Australia*

Junbo Li − *Anhui Province Key Laboratory of Condensed Matter Physics at Extreme Conditions, High Magnetic Field Laboratory, Chinese Academy of Sciences (CAS), Hefei, Anhui 230031, China*

James Partridge − *ARC Centre of Excellence in Future Low-Energy Electronics Technologies (FLEET), School of Science, RMIT University, Melbourne, Victoria 3001, Australia*

Michelle J. S. Spencer − *ARC Centre of Excellence in Future Low-Energy Electronics Technologies (FLEET), School of Science, RMIT University, Melbourne, Victoria 3001, Australia*; orcid.org/0000-0003-4646-1550

Lawrence Farrar − *ARC Centre of Excellence in Future Low-Energy Electronics Technologies (FLEET), School of Science, RMIT University, Melbourne, Victoria 3001, Australia*

Yimin Xiong − *Anhui Province Key Laboratory of Condensed Matter Physics at Extreme Conditions, High Magnetic Field Laboratory, Chinese Academy of Sciences (CAS), Hefei, Anhui 230031, China*

Mingliang Tian − *Anhui Province Key Laboratory of Condensed Matter Physics at Extreme Conditions, High Magnetic Field Laboratory, Chinese Academy of Sciences (CAS), Hefei, Anhui 230031, China; Department of Physics, School of Physics and Materials Science, Anhui University, Hefei, Anhui 230601, China*; orcid.org/0000-0002-0870-995X

Xiaolin Wang − *ARC Centre of Excellence in Future Low-Energy Electronics Technologies (FLEET) and Institute for Superconducting & Electronic Materials, Australian Institute of Innovative Materials, University of Wollongong, Wollongong, New South Wales 2500, Australia*; orcid.org/0000-0003-4150-0848

Complete contact information is available at: https://pubs.acs.org/10.1021/acs.nanolett.2c01370

Author Contributions

#S.A., W.-Q.X., and C.T. contributed equally.

Notes

The authors declare no competing financial interest.

■ ACKNOWLEDGMENTS

This research was performed in part at the RMIT Micro Nano Research Facility (MNRF) in the Victorian Node of the Australian National Fabrication Facility (ANFF) and the RMIT Microscopy and Microanalysis Facility (RMMF). L.W. was supported by the Australian Research Council Centre of Excellence in Future Low-Energy Electronics Technologies (Project No. CE170100039). G.Z. was supported by the 100 Talents Program of Chinese Academy of Sciences (CAS). M.T. was supported by the Natural Science Foundation of China (Grant No. U19A2093). Work at South China University of Technology was supported by the National Natural Science Foundation of China (Grant No. 12074126) and the Key Research and Development Project of Guangdong Province (Grant No. 2020B0303300001).

■ REFERENCES

(1) Kools, J. Exchange-biased spin-valves for magnetic storage. *IEEE Trans. Magn.* **1996**, *32*, 3165−3184.

(2) Nogués, J.; Schuller, I. K. Exchange bias. *J. Magn. Magn. Mater.* **1999**, *192*, 203−232.

(3) Parkin, S. S. P.; Roche, K. P.; Samant, M. G.; Rice, P. M.; Beyers, R. B.; Scheuerlein, R.; O'sullivan, E.; Brown, S.; Bucchigano, J.; Abraham, D.; et al. Exchange-biased magnetic tunnel junctions and application to nonvolatile magnetic random access memory. *J. Appl. Phys.* **1999**, *85*, 5828−5833.

(4) Nogués, J.; Sort, J.; Langlais, V.; Skumryev, V.; Suriñach, S.; Muñoz, J. S.; Baró, M. D. Exchange bias in nanostructures. *Phys. Rep.* **2005**, *422*, 65−117.
(5) Li, K.; Wu, Y.; Guo, Z.; Zheng, Y.; Han, G.; Qiu, J.; Luo, P.; An, L.; Zhou, T. Exchange coupling and its applications in magnetic data storage. *J. Nanosci. Nanotechnol.* **2007**, *7*, 13−45.
(6) Wang, B. M.; Liu, Y.; Ren, P.; Xia, B.; Ruan, K. B.; Yi, J. B.; Ding, J.; Li, X. G.; Wang, L. Large exchange bias after zero-field cooling from an unmagnetized state. *Phys. Rev. Lett.* **2011**, *106*, 077203.
(7) Meiklejohn, W. H.; Bean, C. P. New magnetic anisotropy. *Phys. Rev.* **1956**, *102*, 1413.
(8) Manipatruni, S.; Nikonov, D. E.; Lin, C.-C.; Gosavi, T. A.; Liu, H.; Prasad, B.; Huang, Y.-L.; Bonturim, E.; Ramesh, R.; Young, I. A. Scalable energy-efficient magnetoelectric spin−orbit logic. *Nature* **2019**, *565*, 35−42.
(9) Wu, S. M.; Cybart, S. A.; Yi, D.; Parker, J. M.; Ramesh, R.; Dynes, R. C. Full electric control of exchange bias. *Phys. Rev. Lett.* **2013**, *110*, 067202.
(10) Wu, S. M.; Cybart, S. A.; Yu, P.; Rossell, M. D.; Zhang, J. X.; Ramesh, R.; Dynes, R. C. Reversible electric control of exchange bias in a multiferroic field-effect device. *Nat. Mater.* **2010**, *9*, 756−761.
(11) Borisov, P.; Hochstrat, A.; Chen, X.; Kleemann, W.; Binek, C. Magnetoelectric switching of exchange bias. *Phys. Rev. Lett.* **2005**, *94*, 117203.
(12) He, X.; Wang, Y.; Wu, N.; Caruso, A. N.; Vescovo, E.; Belashchenko, K. D.; Dowben, P. A.; Binek, C. Robust isothermal electric control of exchange bias at room temperature. *Nat. Mater.* **2010**, *9*, 579−585.
(13) Geim, A. K.; Grigorieva, I. V. Van der Waals heterostructures. *Nature* **2013**, *499*, 419−425.
(14) Novoselov, K. S.; Mishchenko, A.; Carvalho, A.; Neto, A. H. C. 2D materials and van der Waals heterostructures. *Science* **2016**, *353*, aac9439.
(15) Liu, Y.; Weiss, N. O.; Duan, X.; Cheng, H.-C.; Huang, Y.; Duan, X. Van der Waals heterostructures and devices. *Nat. Rev. Mater.* **2016**, *1*, 1−17.
(16) Gong, C.; Li, L.; Li, Z.; Ji, H.; Stern, A.; Xia, Y.; Cao, T.; Bao, W.; Wang, C.; Wang, Y.; Qiu, Z. Q.; Cava, R. J.; Louie, S. G.; Xia, J.; Zhang, X. Discovery of intrinsic ferromagnetism in two-dimensional van der Waals crystals. *Nature* **2017**, *546*, 265−269.
(17) Huang, B.; Clark, G.; Navarro-Moratalla, E.; Klein, D. R.; Cheng, R.; Seyler, K. L.; Zhong, D.; Schmidgall, E.; McGuire, M. A.; Cobden, D. H.; Yao, W.; Xiao, D.; Jarillo-Herrero, P.; Xu, X. Layer-dependent ferromagnetism in a van der Waals crystal down to the monolayer limit. *Nature* **2017**, *546*, 270−273.
(18) Gibertini, M.; Koperski, M.; Morpurgo, A. F.; Novoselov, K. S. Magnetic 2D materials and heterostructures. *Nat. Nanotechnol.* **2019**, *14*, 408−419.
(19) Sierra, J. F.; Fabian, J.; Kawakami, R. K.; Roche, S.; Valenzuela, S. O. Van der Waals heterostructures for spintronics and opto-spintronics. *Nat. Nanotechnol.* **2021**, *16*, 856−868.
(20) Tang, W.; Liu, H.; Li, Z.; Pan, A.; Zeng, Y. J. Spin-orbit torque in van der Waals layered materials and heterostructures. *Adv. Sci.* **2021**, *8*, 2100847.
(21) Ohldag, H.; Scholl, A.; Nolting, F.; Arenholz, E.; Maat, S.; Young, A. T.; Carey, M.; Stöhr, J. Correlation between exchange bias and pinned interfacial spins. *Phys. Rev. Lett.* **2003**, *91*, 017203.
(22) Schuller, I. K.; Morales, R.; Batlle, X.; Nowak, U.; Güntherodt, G. Role of the antiferromagnetic bulk spins in exchange bias. *J. Magn. Magn. Mater.* **2016**, *416*, 2−9.
(23) Carpenter, R.; Vallejo-Fernandez, G.; O'Grady, K. Interfacial spin cluster effects in exchange bias systems. *J. Appl. Phys.* **2014**, *115*, 17D715.
(24) O'grady, K.; Fernandez-Outon, L.; Vallejo-Fernandez, G. A. new paradigm for exchange bias in polycrystalline thin films. *J. Magn. Magn. Mater.* **2010**, *322*, 883−899.
(25) Zhu, R.; Zhang, W.; Shen, W.; Wong, P. K. J.; Wang, Q.; Liang, Q.; Tian, Z.; Zhai, Y.; Qiu, C.-w.; Wee, A. T. S. Exchange bias in van der Waals $CrCl_3/Fe_3GeTe_2$ heterostructures. *Nano Lett.* **2020**, *20*, 5030−5035.
(26) Hu, G.; Zhu, Y.; Xiang, J.; Yang, T.-Y.; Huang, M.; Wang, Z.; Wang, Z.; Liu, P.; Zhang, Y.; Feng, C.; Hou, D.; Zhu, W.; Gu, M.; Hsu, C.-H.; Chuang, F.-C.; Lu, Y.; Xiang, B.; Chueh, Y.-L. Antisymmetric magnetoresistance in a van der Waals antiferromagnetic/ferromagnetic layered $MnPS_3/Fe_3GeTe_2$ stacking heterostructure. *ACS Nano* **2020**, *14*, 12037−12044.
(27) Dai, H.; Cheng, H.; Cai, M.; Hao, Q.; Xing, Y.; Chen, H.; Chen, X.; Wang, X.; Han, J.-B. Enhancement of the coercive field and exchange bias effect in $Fe_3GeTe_2/MnPX_3$ (X= S and Se) van der Waals heterostructures. *ACS Appl. Mater. Interfaces* **2021**, *13*, 24314−24320.
(28) Zhang, L.; Huang, X.; Dai, H.; Wang, M.; Cheng, H.; Tong, L.; Li, Z.; Han, X.; Wang, X.; Ye, L.; Han, J. Proximity-coupling-induced significant enhancement of coercive field and Curie temperature in 2D van der Waals heterostructures. *Adv. Mater.* **2020**, *32*, 2002032.
(29) Wu, Y.; Wang, W.; Pan, L.; Wang, K. L. Manipulating exchange bias in a van der Waals ferromagnet. *Adv. Mater.* **2022**, *34*, 2105266.
(30) Zhuo, W.; Lei, B.; Wu, S.; Yu, F.; Zhu, C.; Cui, J.; Sun, Z.; Ma, D.; Shi, M.; Wang, H.; Wang, W.; Wu, T.; Ying, J.; Wu, S.; Wang, Z.; Chen, X. Manipulating ferromagnetism in few-layered $Cr_2Ge_2Te_6$. *Adv. Mater.* **2021**, *33*, 2008586.
(31) Zheng, G.; Xie, W.-Q.; Albarakati, S.; Algarni, M.; Tan, C.; Wang, Y.; Peng, J.; Partridge, J.; Farrar, L.; Yi, J.; Xiong, Y.; Tian, M.; Zhao, Y.-J.; Wang, L. Gate-tuned interlayer coupling in van der Waals ferromagnet Fe_3GeTe_2 nanoflakes. *Phys. Rev. Lett.* **2020**, *125*, 047202.
(32) Tan, C.; Xie, W.-Q.; Zheng, G.; Aloufi, N.; Albarakati, S.; Algarni, M.; Li, J.; Partridge, J.; Culcer, D.; Wang, X.; Yi, J. B.; Tian, M.; Xiong, Y.; Zhao, Y.-J.; Wang, L. Gate-controlled magnetic phase transition in a van der Waals magnet Fe_3GeTe_2. *Nano Lett.* **2021**, *21*, 5599−5605.
(33) May, A. F.; Ovchinnikov, D.; Zheng, Q.; Hermann, R.; Calder, S.; Huang, B.; Fei, Z.; Liu, Y.; Xu, X.; McGuire, M. A. Ferromagnetism near room temperature in the cleavable van der Waals crystal Fe_5GeTe_2. *ACS Nano* **2019**, *13*, 4436−4442.
(34) Joy, P.; Vasudevan, S. Magnetism in the layered transition-metal thiophosphates MPS_3 (M= Mn, Fe, and Ni). *Phys. Rev. B* **1992**, *46*, 5425.
(35) Lee, J.-U.; Lee, S.; Ryoo, J. H.; Kang, S.; Kim, T. Y.; Kim, P.; Park, C.-H.; Park, J.-G.; Cheong, H. Ising-type magnetic ordering in atomically thin $FePS_3$. *Nano Lett.* **2016**, *16*, 7433−7438.
(36) Hohenberg, P.; Kohn, W. Density functional theory (DFT). *Phys. Rev.* **1964**, *136*, B864.
(37) Kohn, W.; Sham, L. J. Self-consistent equations including exchange and correlation effects. *Phys. Rev.* **1965**, *140*, A1133.
(38) Nogués, J.; Leighton, C.; Schuller, I. K. Correlation between antiferromagnetic interface coupling and positive exchange bias. *Phys. Rev. B* **2000**, *61*, 1315.
(39) Malozemoff, A. Random-field model of exchange anisotropy at rough ferromagnetic-antiferromagnetic interfaces. *Phys. Rev. B* **1987**, *35*, 3679.
(40) Ishiwata, S.; Taguchi, Y.; Murakawa, H.; Onose, Y.; Tokura, Y. Low-magnetic-field control of electric polarization vector in a helimagnet. *Science* **2008**, *319*, 1643−1646.

https://doi.org/10.1021/acs.nanolett.2c01370
Nano Lett. 2022, 22, 6166−6172